

Diamagnetic nature of stratified thin metals in visible range

Masanobu Iwanaga*

Department of Physics, Graduate School of Science, Tohoku University, Sendai 980-8578, Japan

(Dated: November 9, 2019)

It is numerically demonstrated that effectively strong diamagnetic resonance emerges at visible frequencies in stratified metal-dielectric metamaterials. The effective optical constants are extracted by two complex reflectivity method. It is clarified that the effective diamagnetic response originates from stratified layers of thin metals and is always associated with effective plasma frequency. The diamagnetic response is therefore ascribed to a magnetic component of the collective excitation. The diamagnetism is crucially sensitive to the mesoscopic structure including the surface layer.

PACS numbers: 42.25.Bs, 42.70.Qs, 78.20.Ci, 73.22.Lp

Photonic metamaterials are trials to invent and produce novel electromagnetic (EM) states by modifying periodic structures in which constituents have the same optical constants with bulk materials. The trials start at gigahertz and proceed to terahertz and optical frequencies with remarkable progress reviewed in Refs. [1, 2]. The strategy is significantly different from nano-scale materials science in which quantum size effect on electronic states is a key. In metamaterials, novel effective EM states are explored by controlling the geometrical structures. The effective EM states are solutions of Maxwell equations for a homogenized system obtained by coarse-graining and represents averaged EM fields approximately.

Recent metamaterial optics usually employs a retrieval way for evaluation of effective optical constants [3]. The way is algorithmic and not rigorous compared with the effective media description, which has been studied over one century [4, 5, 6] since Maxwell-Garnet [7]. The effective media descriptions are usually derived for specified structures by assuming analytical models and the long wavelength limit. The difference between the effective media description and recent retrieval way was already described in the introduction of Ref. [3]. In short, the effective media description is derived analytically for ideally large objects under the long wavelength approximation, while the retrieval way analyzes complex transmissivity and reflectivity (called S parameters) in evaluating effective optical constants in an algorithmic way. In the latter, there are two distinct points from the former: (i) the interface of metamaterials play a crucial role because the S parameters are sensitive to the surface layers; (ii) the description using effective optical constants turned out to be approximately valid for several artificial metamaterials beyond the long wavelength limit [3].

By use of the retrieval way, effective magnetic responses and negative refraction at optical frequencies have been demonstrated experimentally [8, 9, 10]. Those metamaterials become candidates to be exceptions to the statement, by Landau and Lifshitz, that permeability is

unity at optical frequencies [11].

A simple theoretical analysis presented a possibility of negative refractive index in a thin metal film [12] and the sub-diffraction-limited image was shown experimentally [13]. It is expected that near-EM-field enhancement is induced to compensate the loss at resonance with exploiting thin metallic layers. Another experimental result on transmission was reported which supports the enhancement of EM fields by stratified thin metals [14]. It was also shown that the enhancement is associated with high magnetic field in thin metals [15]. Besides, it was very recently argued that negative refractive response appears in stratified stacks composed of metal-dielectric several layers [16]. Thus, the magnetic response in metallic thin films attracts great interest, connecting to optics with negative refraction.

In the present Communication, stratified metal-dielectric metamaterials (SMDM) are specified to examine effective magnetic response at visible frequencies. Figure 1 shows the schematic drawing of SMDM and the coordinate configuration. Since the structure is uniaxial, effective tensors of permittivity ε and permeability μ are

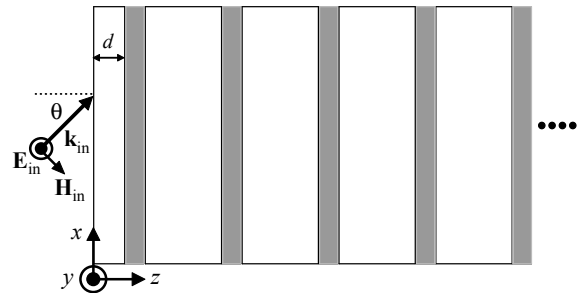


FIG. 1: Schematic drawing for structure of SMDM and coordinate configuration. Gray indicates metal (Ag) and white dielectric (MgF_2). The thickness of surface layer is denoted by d . Incident light sheds on xy plane with s polarization (*i.e.* $\mathbf{E}_{\text{in}} \parallel y$) and incident angle θ . In this configuration, the two products of ε_y/μ_x and $\mu_x\mu_z$ are determined uniquely from two incident angles.

*Electronic address: M.Iwanaga@osa.org

assumed to be diagonal and uniaxial:

$$\varepsilon = \begin{pmatrix} \varepsilon_x & 0 & 0 \\ 0 & \varepsilon_y & 0 \\ 0 & 0 & \varepsilon_z \end{pmatrix}, \quad \mu = \begin{pmatrix} \mu_x & 0 & 0 \\ 0 & \mu_y & 0 \\ 0 & 0 & \mu_z \end{pmatrix}. \quad (1)$$

The tensors are also assumed to describe local EM responses. The optical axis is set to be the z axis, and then the two relations of $\varepsilon_x = \varepsilon_y$ and $\mu_x = \mu_y$ hold in Eq. (1). The periodicity is set to be 75 nm. The thickness of metal (Ag) and dielectric (MgF₂) are 15 and 60 nm, respectively. The thickness of Ag layers was set to ensure using dielectric constant of bulk silver in literature [17].

In this study, bulk SMDM is analyzed which is thick enough to eliminate transmission, and full components of ε and μ tensors are extracted by two complex reflectivity method (TCRM). Although the method and numerical details were described already [18], we briefly survey the scheme in the following. Complex reflectivity r_s under s polarization (that is, $\mathbf{E}_{\text{in}}||y$) in Fig. 1 satisfies at the interface:

$$\frac{\hat{k}_z(\theta)}{\mu_x} = \frac{n_0 \cos \theta}{\mu_0} \cdot \frac{1 - r_s(\theta)}{1 + r_s(\theta)}. \quad (2)$$

where $\hat{k}_z(\theta)$ is the z component of refractive wavenumber vector normalized by wavenumber k_0 in vacuum; in particular, $\hat{k}_z(0)$ is refractive index along the z axis. Besides, n_0 and μ_0 denote the refractive index and permeability in vacuum. Equation of dispersion under s polarization is written as

$$\varepsilon_y = \frac{\hat{k}_z(\theta)^2}{\mu_x} + \frac{\hat{k}_x(\theta)^2}{\mu_z}, \quad (3)$$

where $\hat{k}_x(\theta) = n_0 \sin \theta$ in the configuration of Fig. 1. Setting the right hand side of Eq. (2) to be $f_s(\theta)$ and combining Eqs. (2) and (3), we obtain the next equation:

$$\frac{\varepsilon_y}{\mu_x} = f_s^2(\theta) + \frac{n_0^2 \sin^2 \theta}{\mu_x \mu_z}. \quad (4)$$

Two different angles ($\theta_1 \neq \theta_2$) yield $\sin \theta_1 \neq \sin \theta_2$, and enable to evaluate ε_y/μ_x and $\mu_x \mu_z$ uniquely. By permutating the configuration (x, y, z) \rightarrow (y, z, x), we can figure ε_z/μ_y and $\mu_y \mu_x$. Since the relations of $\varepsilon_x = \varepsilon_y$ and $\mu_x = \mu_y$ are assumed for SMDM, μ_x^2 is evaluated; succeedingly, the rest components of μ_z , ε_x , and ε_z are uniquely obtained except for the sign. The sign of μ_x is set to be $\mu_x \approx 1$ at off-resonance of 800 nm and is identified without discontinuous jump as shown in Fig. 2. The precision in the computation for r_s ensures that the full components of tensors are determined within a few-percent numerical error.

Figure 2 presents the full components of (a) ε and (b) μ tensors extracted by TCRM with the two angles of 0° and 15°. Other sets of two incident angles (0° and $\theta \neq 0^\circ$) result in the same spectra of ε_x , ε_z , and μ_x within a numerical error. In TCRM analysis using Eq. (4) and

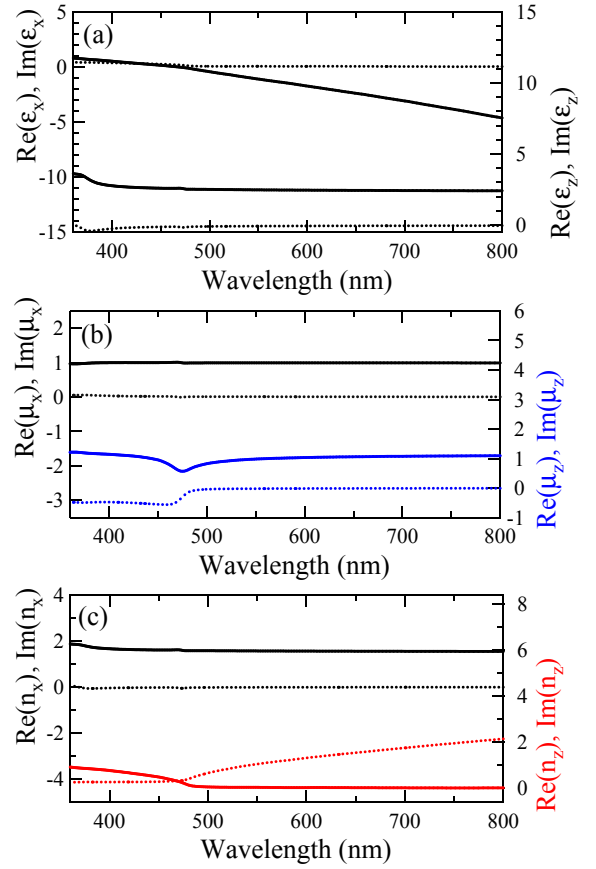


FIG. 2: Effective optical constants of SMDM, extracted with the two incident angles of 0° and 15°. (a): Effective permittivity. Upper solid line denotes $\text{Re}(\varepsilon_x)$ and upper dotted line does $\text{Im}(\varepsilon_x)$. Lower two lines represent ε_z likewise. (b): Effective permeability. Lines indicate μ_x and μ_z with the notation similar to (a). (c): Effective refractive index along the x and z axes. The real parts are shown with solid lines and the imaginary parts with dotted lines.

the angle pair ($0^\circ, \theta$), it is easily found that μ_z depends only on the θ in Fig. 1; therefore, we can extract $\mu_z(\theta)$ at oblique angle. Thus, all the components of ε and μ tensors are determined in a well-defined manner at visible frequencies in Fig. 2.

The ε_x component has typical dispersion of Drude metal (upper solid and dotted lines in Fig. 2(a): the real and imaginary parts of ε_x , respectively), and the effective plasma frequency $\omega_{p,\text{eff}}$, which is defined by $\text{Re}(\varepsilon_x(\omega_{p,\text{eff}})) = 0$, is located at $\lambda_{p,\text{eff}} = c/2\pi\omega_{p,\text{eff}} = 468$ nm. On the other hand, the ε_z spectrum exhibits typical dielectric properties for the incident light of $\mathbf{E}_{\text{in}}||z$ on the xz or yz planes (lower solid and dotted lines in Fig. 2(a): the real and imaginary parts of ε_z , respectively). Concerning permeability components, μ_x is close to 1 at 360–800 nm (upper solid and dotted lines in Fig. 2(b): the real and imaginary parts of μ_x , respectively), while μ_z goes down to 0.57 at 477 nm and shows strong diamagnetism (lower solid and dotted lines in Fig. 2(b): the real and imaginary parts of μ_z , respectively). Refrac-

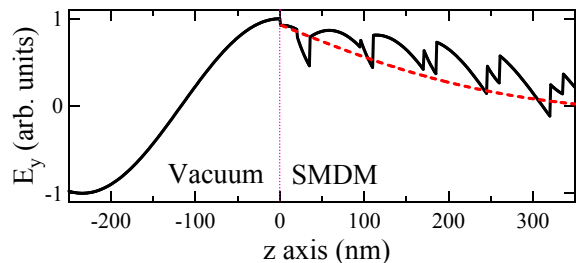


FIG. 3: Electric field vs the averaged field. Electric field is calculated at $\lambda_{p,eff}$ under normal incidence on the xy plane with s polarization. Solid line indicates forward propagation only, that is, incident and refractive components. Dashed line represents the electric field calculated by the effective refractive index n_z in Fig. 2(c). Vertical dotted line indicates the interface.

tive indexes along the x and z axes are displayed in Fig. 2(c); the upper solid and dotted lines respectively denote $\text{Re}(n_x)$ and $\text{Im}(n_x)$, and the lower solid and dotted lines respectively stand for $\text{Re}(n_z)$ and $\text{Im}(n_z)$. The imaginary parts of n_x and n_z are small below $\lambda_{p,eff}$, and correspond to efficient EM-wave propagation.

In Fig. 3, we examine the validity of description by effective refractive index at $\lambda_{p,eff}$. The interface of vacuum and SMDM is set at $z = 0$ and incident light illuminates on the xy plane normally. Solid line denotes electric field of incident light in vacuum ($z < 0$); it represents refractive component of electric field in SMDM ($z > 0$). Dashed line presents the effective field profile calculated by using n_z in Fig. 2(c) and reproduces the averaged field profile in SMDM approximately. Thus, TCRM extracts averaged EM response in SMDM. As was confirmed in Ref. [18], the effective description has relevant physical meanings and works fairly well in the visible range of interest.

As shown in Fig. 2, diamagnetic response is detected in μ_z . This implies that magnetic induction B_z and magnetic field H_z behave in a different way. Figure 4 displays the image plot of (a) B_z and (b) H_z at 477 nm, the minimum of $\text{Re}(\mu_z)$. Arrows denote the vectors at dotted points. In vacuum ($z < 0$), the incident light travels with incident angle 15° , whereas in SMDM ($z > 0$) both forward and backward components are displayed simultaneously because reflectance R is not small ($R \sim 0.7$) and the backward components connected to inner multi-reflection is not negligible. When the EM fields are monochromatic plane waves and proportional to $\exp(i\mathbf{k} \cdot \mathbf{r} - i\omega t)$, the computation for B_z is carried out from one of Maxwell equations:

$$i\omega\mathbf{B} = i\mathbf{k} \times \mathbf{E}. \quad (5)$$

Magnetic field H_z is also calculated from

$$i\mathbf{k} \times \mathbf{H} = -i\omega\mathbf{D}. \quad (6)$$

Figure 4 obviously shows that the directions of B_z and H_z are opposite in metallic layer ($20 < z < 35$ nm). Di-

electric layers behave like paramagnetic materials. Besides, the H_z component in the metallic layer is far more intense than the H_z in vacuum and dielectric layers. In this way, the metallic layers act as if they are diamagnetic materials. The diamagnetic nature does not come from electronic spin states of silver but from superimposed EM fields in mesoscopic structure of SMDM. The backward component is indeed responsible for the diamagnetic response. The diamagnetic response is found to come from the thin metallic layers and is indeed extracted by using effective optical constants. We can thus draw a concise picture by effective description.

Figure 5 shows the dependence of μ_z on incident angle. In employing the two angles of 0° and $\theta (\neq 0^\circ)$, the extracted μ_z depends only on the θ in Fig. 1, as is easily verified from Eq. (4). The other components (μ_x , ε_x , and ε_z) are almost independent of θ . Therefore, the μ_z spectra in Fig. 5 can be interpreted as the indication of spatial dispersion, that is, $\mu_z = \mu_z(\mathbf{k})$ where \mathbf{k} is the wavenumber vector in SMDM. Note that μ_z at off-resonance above 540 nm is almost independent of θ and the spatial dispersion is a resonant behavior.

Figure 6 displays the effect of surface layer on the effective μ_z . Figures 2–5 are the results regarding the surface thickness $d = 20$ nm; the spectra is shown again in Fig. 6. From bottom to top, the thickness d varies from 0 to 30 nm, respectively. SMDM with $d = 0$ and 10 nm show diamagnetic property in a wide range. The increase of surface thickness d gradually cancels diamagnetic response and finally eliminates the diamagnetism at $d = 30$ nm. Since the surface layer directly affects the phase of EM wave in SMDM, it is crucially significant how to set the surface layer in realizing the diamagnetism. Figure

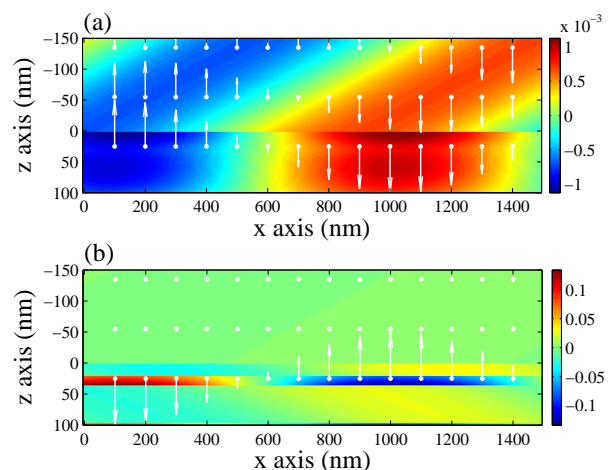


FIG. 4: Comparison of (a) B_z and (b) H_z at 477 nm, the minimum of $\text{Re}(\mu_z)$. The region of vacuum ($z < 0$) for simplicity shows incident light and incident angle $\theta = 15^\circ$, and that of SMDM ($z > 0$) contains both forwardly and backwardly propagating components. Arrows indicate the vectors at typical points (dots). In particular, the directions of B_z and H_z in metallic layer ($20 < z < 35$ nm) are clearly opposite.

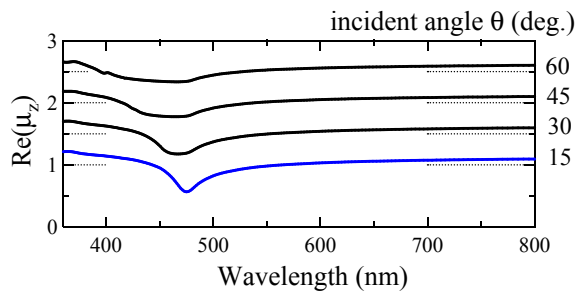


FIG. 5: Spatially dispersive behavior of μ_z resonance. All the spectra are obtained by TCRM with the two angles of 0° and $\theta (\neq 0^\circ)$. However, as described in the text, μ_z depends only on the θ in Fig. 1. The spectrum at 15° is the same with that in Fig. 2(b). The spectra at $\theta = 30^\circ, 45^\circ$, and 60° are offset for visibility by 0.5, 1.0, and 1.5, respectively. Horizontal dotted lines indicate $\text{Re}(\mu_z) = 1.0$ for each spectrum.

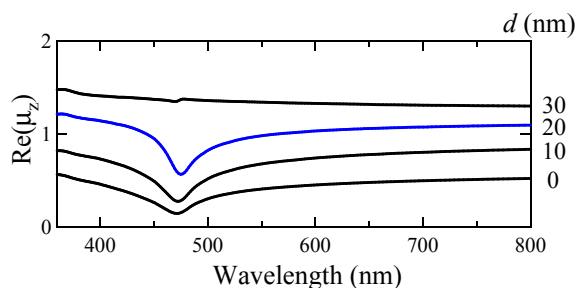


FIG. 6: Permeability μ_z spectra of SMDM with various surface layers: the thickness d of surface layers from 0 to 30 nm. All the spectra are determined with the two incident angles of 0° and 15° , and are presented without vertical offset. The spectrum of $d = 20$ nm in Fig. 5 is displayed again for comparison.

6 is the explicit indication. It is consistent with the conclusion in a recent numerical study [19], showing that the interfaces play a vital role in photonic slabs of finite thickness, in extracting effective constants by the retrieval way.

As is shown in Figs. 4 and 6, the effective diamagnetic response emerges at about $\lambda_{p,\text{eff}}$, comes from the stratified metallic layers, and is sensitive to the surface layer in SMDM. In other words, to detect the diamagnetic resonance from the outside of SMDM, it is essential how to select both the structure of unitcell and the sur-

face layer. As the $\lambda_{p,\text{eff}}$ shifts with varying the ratio of metal in the unitcell, the diamagnetic resonance follows the shift of $\lambda_{p,\text{eff}}$. It indicates that the diamagnetic resonance is magnetic part of the effective plasma resonance. The spatially dispersive behavior in Fig. 5 also supports the connection to the plasma resonance.

From computational and theoretical studies, it was reported that magnetism takes place in the systems composed of dielectric [6, 20] and metallic rods [21, 22], comes from the Mie resonances peculiar to the rods, and is spatially dispersive [6, 21]. These magnetic responses come from the resonance due to geometrical shape of constituents; in this viewpoint, there is similarity to SMDM.

Thick enough SMDM have been focused on in this Communication. Of course, this system is not easily fabricated in reality. However, it is a good touchstone to examine how the effective optical responses emerge in periodic metal-dielectric systems. In the present analysis, there is no evidence to suggest negative refraction in SMDM, which was lately argued in finite systems [16]. If negative refraction took place in finitely thick SMDM, it should be due to an interference effect in finite systems.

In conclusion, the full components of effective tensors of ε and μ in SMDM has been numerically extracted by TCRM in a well-defined way. As a result, the effective diamagnetic resonance along the optical axis has been clarified. The diamagnetism results from the EM response in the stratified mesoscopic structure including the surface layer. It has shown that stratified metals act as source of diamagnetism. The diamagnetic resonance is induced always near the effective plasma frequency; therefore, it can be regarded as a magnetic component of the collective excitation. The diamagnetic nature of thin metals is experimentally feasible, and it will be a good test to measure nonlinear optical processes via diamagnetic resonance.

Acknowledgments

The author thanks T. Ishihara and S. G. Tikhodeev for stimulating discussion. This study was partially supported by Research Foundation for Opto-Science and Technology and by the Information Synergy Center, Tohoku University in numerical implementation.

-
- [1] J. B. Pendry and D. R. Smith, *Phys. Today* **57**(6), 37 (2004).
 - [2] V. M. Shalaev, *Nature Photon.* **1**, 41 (2007).
 - [3] D. R. Smith, D. C. Vier, T. Koschny, and C. M. Soukoulis, *Phys. Rev. E* **71**, 036617 (2005), and earlier references cited therein.
 - [4] W. Lamb, D. M. Wood, and N. W. Ashcroft, *Phys. Rev. B* **21**, 2248 (1980), and earlier references cited therein.
 - [5] D. J. Bergman, *Phys. Rev. Lett.* **44**, 1285 (1980); *ibid* **45**, 148 (1980).
 - [6] D. Felbacq and G. Bouchitté, *Phys. Rev. Lett.* **94**, 183902 (2005), and earlier references cited therein.
 - [7] J. C. Maxwell-Garnet, *Philos. Trans. R. Soc. London* **203**, 385 (1904); *ibid.*, **205**, 237 (1906).
 - [8] S. Zhang, W. Fan, N. C. Panoiu, K. J. Malloy, R. M. Osgood, and S. R. J. Brueck, *Phys. Rev. Lett.* **95**, 137404

- (2005).
- [9] V. M. Shalaev, W. Cai, U. K. Chettiar, H.-K. Yuan, A. K. Sarychev, V. P. Drachev, and A. V. Kildishev, *Opt. Lett.* **30**, 3356 (2005).
 - [10] G. Dolling, C. Enkrich, M. Wegener, C. M. Soukoulis, and S. Linden, *Opt. Lett.* **31**, 1800 (2006).
 - [11] L. D. Landau and E. M. Lifshitz, *Electrodynamics of Continuous Media* (Pergamon, New York, 1984), 2nd ed.
 - [12] J. B. Pendry, *Phys. Rev. Lett.* **85**, 3966 (2000).
 - [13] N. Fang, H. Lee, C. Sun, and X. Zhang, *Science* **305**, 534 (2005).
 - [14] M. Scalora, M. J. Bloemer, A. S. Manka, S. D. Pethel, J. P. Dowling, and C. M. Bowden, *J. Appl. Phys.* **83**, 2377 (1998).
 - [15] L. Zhou, W. Wen, C. T. Chan, and P. Sheng, *Phys. Rev. Lett.* **94**, 243905 (2005).
 - [16] M. Scalora, G. D'Aguanno, N. Mattiucci, M. J. Bloemer, D. de Ceglia, M. Centini, C. Sibilia, N. Akozbek, M. G. Cappeddu, M. Fowler, et al., *Opt. Express* **15**, 508 (2007).
 - [17] P. B. Johnson and R. W. Christy, *Phys. Rev. B* **6**, 4370 (1972).
 - [18] M. Iwanaga, *Opt. Lett.* (to be published), posted as Doc. ID 78547.
 - [19] T. Decoopman, G. Tayeb, S. Enoch, D. Maystre, and B. Gralak, *Phys. Rev. Lett.* **97**, 073905 (2006).
 - [20] K. C. Huang, M. L. Povinelli, and J. D. Joannopoulos, *Appl. Phys. Lett.* **85**, 543 (2004).
 - [21] D. Felbacq and G. Bouchitté, *Opt. Lett.* **30**, 1189 (2005).
 - [22] X. Hu, C. T. Chan, J. Zi, M. Li, and K. M. Ho, *Phys. Rev. Lett.* **96**, 223901 (2006).